ISSN 0038-0946, Solar System Research, 2007, Vol. 41, No. 3, pp. 177–185. © Pleiades Publishing, Inc., 2007.
Original Russian Text © Yu.G. Shkuratov, V.G. Kaydash, L.V. Starukhina, C.M. Pieters, 2007, published in Astronomicheskii Vestnik, 2007, Vol. 41, No. 3, pp. 195–203.

Lunar Surface Agglutinates: Mapping Composition Anomalies

Yu. G. Shkuratov[a], V. G. Kaydash[a], L. V. Starukhina[a], and C. M. Pieters[b]

[a] *Institute of Astronomy, Kharkov National University, Sumskaya ul. 35, Kharkov, 61022 Ukraine*

[b] *Department of Geological Sciences, Brown University, Providence, RI, 02912 USA*

Received April 27, 2006; in final form, June 20, 2006

Abstract—From the *Clementine* UVVIS imagery of the lunar surface, the abundance of agglutinates in the lunar regolith and their composition in terms of FeO and Al_2O_3 oxides have been predicted. Data on the spectral, chemical, and mineralogic measurements of about 30 lunar soil samples from the Lunar Samples Characterization Consortium (LSCC) collection were used. The fulfilled prognosis confirms that the mare agglutinates are enriched in Al_2O_3 and depleted of FeO, while the highland agglutinates are depleted of Al_2O_3 and enriched in FeO. This behavior can be caused by the global transport of the lunar surface material induced by cosmogenic factors.

PACS: 96.15.-n, 96.25.Hs

DOI: 10.1134/S003809460703001X

INTRODUCTION

Agglutinates are the most altered portion of lunar surface material. Agglutinate particles are debris of rocks and minerals consolidated by glasses produced by micrometeoritic impacts (e.g., Rode et al., 1979). Although the composition of agglutinate particles mostly corresponds to that of the local material, exceptions are frequently observed. It is important to study the causes of these exceptions because this can elucidate the evolution of the lunar surface and, in particular, provide information about the efficiency of the global material transport on this surface (Pieters and Taylor, 2003). The lunar soil contains several tens of percent of agglutinates (McKay et al., 1991). In mature soil, the abundance of agglutinates is several times higher than in immature soil.

Analysis of lunar soil samples showed that, relative to the crystalline fraction, the mare agglutinates are enriched in Al and depleted of Fe, Ti, and Cr, while the highland agglutinates are vice versa, depleted of Al and enriched in Fe, Ti, and Cr (Pieters and Taylor, 2003). In the present study, we confirm the effect found in the samples and extend the result for Al and Fe to the whole lunar surface. We also consider the mechanisms of the global maria–highlands exchange of material, which can explain this effect.

In its technique and problem statement, the present paper continues the studies initiated by Shkuratov et al. (2003, 2005a, 2005b) and Pieters et al. (2006). As before, we use data of the spectral, chemical, and mineral studies of lunar samples of fine-grained fractions determining the optical properties of the lunar surface. Some results of the analysis of the mutual correlations between the abundances of the main chemical elements have been described by Pieters et al. (2002, 2006) and Shkuratov et al. (2005a).

The available data allow us to predict not only the chemical and mineral composition of lunar soil in general, but also to study the composition of its mineral components with the use of the images obtained by the *Clementine* spacecraft. We have already attempted to map the composition of lunar pyroxenes (Shkuratov et al., 2005b). In the present paper, we use the same technique to map the composition of lunar agglutinates.

INITIAL DATA AND MAPPING TECHNIQUE

To map the composition of lunar agglutinates, we used the *Clementine* UVVIS imagery in five wavelengths of the visible and near-IR spectral ranges (McEwen et al., 1998). The images are 1-km-resolution mosaics. Additionally, we used data of the spectral, chemical, and mineral studies carried out by the LSCC research consortium (Taylor et al., 2001, 2003) investigating the lunar regolith. The mosaics are composed of many strips approximately 30 km wide stretching from the southern to the northern pole of the Moon (along the spacecraft trajectory). The strips are not only well coregistered geometrically, but also thoroughly adjusted photometrically. The spectral measurements of the samples were made with the RELAB spectrometer in the 0.35–2.5 μm spectral range (Pieters and Hiroi, 2004). It is of principal importance that data from the *Clementine* imagery and the RELAB spectral measurements are reduced to the same photometric system.

Figure 1 shows an example of the albedo mosaic (the wavelength is 900 nm); the images of the Moon at

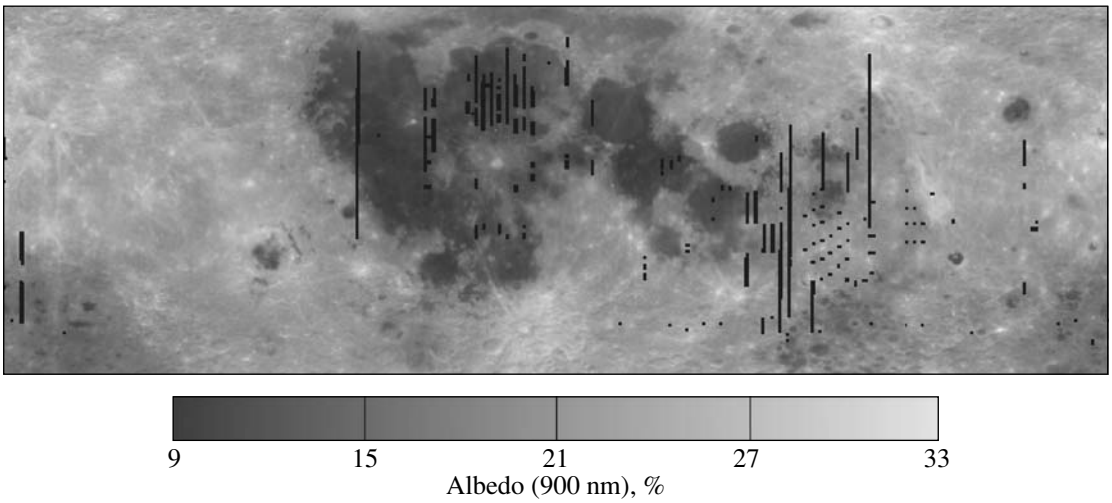

Fig. 1. The albedo distribution (900 nm) over the lunar surface from the UVVIS/*Clementine* data. In the map, dark vertical strips correspond to the regions that were not covered by imaging.

different wavelengths are almost identical in appearance. Dark vertical strips in the figure correspond to the regions not covered by imaging. The mosaic is given in cylindrical projection. The near-pole regions are removed from the images, because they were imaged at grazing solar illumination, when the topography prevents a reliable analysis.

To predict the composition of the lunar surface, we used about 30 samples of the highland and mare regolith. Among them, there are bulk samples and their size fractions with grains smaller than 45 μm, from 20 to 45 μm, from 10 to 20 μm, and smaller than 20 μm (see Shkuratov et al. (2003, 2005b) and Pieters et al. (2006) for details). In Table 1, we provide information on the samples, the albedo values for the UVVIS/*Clementine* spectral bands, the agglutinate abundances, the bulk contents of some oxides in the sample, and the content of these oxides in agglutinates. These data were used to map the predicted composition of the lunar soil and the predicted composition of agglutinates in the lunar soil. For this, it was necessary to find such a combination of the spectral albedo values that produces the closest correlation with the measured and predicted values of a given chemical parameter for the lunar soil samples. As in our previous studies (Shkuratov et al., 2003, 2005b; Pieters et al., 2006), we compared several different combinations of the spectral albedo A in order to obtain high correlation coefficients. The simple linear combination of the albedo values at four wavelengths (λ = 415, 750, 900, and 1000 nm) turned out to be the best:

$$\log(P) = aA_{415} + bA_{750} + cA_{900} + dA_{1000} + e. \quad (1)$$

The logarithm is used in formula (1) in order to avoid negative values of the predicted parameter P. The closest correlation between the predicted and measured values of the parameter P is obtained by varying the coefficients a, b, c, d, and e in Eq. (1). The coefficients, at which the highest correlation is obtained in the case of the prognosis of agglutinate abundances, are given in Table 2 (albedos should be expressed in percentages). This table also contains the correlation coefficient for the predicted and measured abundances of agglutinates. Although this coefficient is rather high (k = 0.84), it is somewhat lower than that for the maturity degree I_s/FeO (k = 0.88) (Kaydash et al., 2004). The coefficients of correlation between the measured and predicted values of the bulk content of some oxides and the content of the same oxides in agglutinates are listed in Table 3. The highest values of the correlation coefficient are observed for CaO oxide; the lowest values are for titanium dioxide. We study FeO and Al_2O_3 oxides in the context of the composition anomalies found by Pieters and Taylor (2003). Table 4 lists the values of a, b, c, d, and e for Eq. (1), at which the correlation coefficients given in Table 3 are obtained for FeO and Al_2O_3. The data for these oxides are presented both for the lunar soil without its separation into components (the bulk composition) and individually for its agglutinate component. Figure 2 shows the correlation diagrams for the measured and predicted quantities of the agglutinate abundance as well as for the iron and aluminum contents in agglutinates. These diagrams and the relatively high correlation coefficients (Table 3) show that the content of FeO and Al_2O_3 can be predicted rather reliably. The error in the prognosis can be estimated by the scattering of the points in the diagrams displayed in Fig. 2. With the albedo mosaics and with the coefficients for Eq. (1) from Tables 2 and 4, the prognosis maps of the corresponding parameters can be built.

Table 1. Data for the lunar soil samples used in this study

Samples	415 nm	750 nm	900 nm	950 nm	1000 nm	Agglutinates, mass %	TiO_2 agglutinates	Al_2O_3 agglutinates	FeO agglutinates	SiO_2 agglutinates	MgO agglutinates	CaO agglutinates	TiO_2	Al_2O_3	FeO	SiO_2	MgO	CaO
10084	0.046	0.08	0.09	0.093	0.096	62.57	2.06	10.26	7.38	27.84	5.43	8.26	7.386	16.2	12.22	42.89	7.335	12.53
10084	0.043	0.069	0.075	0.075	0.077	57.02	1.68	10.26	5.82	25.77	4.82	7.93	8.091	13.45	14.98	41.99	8.132	12.02
10084	0.044	0.065	0.064	0.063	0.063	53.87	1.59	9.37	5.71	23.97	4.68	7.11	8.429	12.19	15.74	41.94	8.591	11.78
12001	0.046	0.076	0.072	0.07	0.073	56.15	1.27	8.42	7.3	26.22	4.81	6.68	3.252	11.18	17.18	46.04	10.77	9.991
12030	0.099	0.154	0.135	0.13	0.136	49.77	1.21	6.62	6.77	23.74	4.46	5.77	3.361	10.83	17.41	46.88	9.983	9.76
12030	0.099	0.148	0.122	0.116	0.12	39.39	1.08	5.24	5.4	18.83	3.44	4.57	3.794	10.65	17.85	46.76	10.08	9.221
14141	0.136	0.201	0.16	0.157	0.173	40.96	0.75	7.33	4	19.25	3.27	4.67	1.96	15	11.6	47.2	11	10.1
14141	0.169	0.259	0.24	0.239	0.257	48.63	0.82	9.39	4.28	22.76	3.85	5.79	1.71	17.2	9.46	48.4	9.08	10.7
14163	0.061	0.102	0.094	0.094	0.101	56.44	0.97	9.71	5.76	26.41	4.88	6.43	2	15.4	11.5	47.1	11	10.2
14163	0.08	0.139	0.144	0.146	0.155	58.46	0.97	10.58	5.64	27.13	5.05	6.78	1.88	17	10.1	47.4	9.57	10.8
14259	0.049	0.081	0.082	0.083	0.088	60.53	0.91	11.62	5.55	28.17	5.07	7.26	1.99	15.8	11	47.1	10.7	10.5
14259	0.059	0.119	0.13	0.135	0.143	68.73	1.13	12.85	6.74	31.48	5.73	8.11	1.96	17.4	9.71	47.5	9.44	11
14260	0.046	0.079	0.079	0.08	0.085	64.04	0.99	11.91	6.17	29.65	5.39	7.43	1.86	16.3	10.7	47.4	10.4	10.7
14260	0.057	0.119	0.129	0.133	0.141	65.19	1.06	12.97	5.77	29.66	5.47	8.08	1.98	17.3	9.84	47.5	9.53	11
15041	0.042	0.076	0.079	0.079	0.083	56.68	0.8	9.52	6.46	26.7	5.54	6.52	1.908	13.7	14.61	46.88	10.96	10.35
15041	0.046	0.076	0.073	0.073	0.076	51.28	0.69	9.13	5.69	23.79	4.82	6.2	2.064	12.71	15.46	46.87	11.39	10.08
15071	0.047	0.088	0.088	0.088	0.092	49.17	0.78	8.06	6.05	22.72	5.11	5.65	1.905	13.07	15.6	46.31	11.15	10.34
15071	0.05	0.085	0.08	0.08	0.084	47.63	0.7	7.81	5.86	22.1	4.63	5.48	2.36	12.56	15.8	46.39	11.55	9.936
61141	0.076	0.127	0.135	0.139	0.145	50.08	0.53	11.77	3.59	22.14	3.77	7.16	0.58	26.1	5.15	44.5	6.56	15.2
61221	0.231	0.3	0.268	0.263	0.27	28.92	0.32	7	1.8	13.04	1.9	4.14	0.49	28.25	4.55	45.35	5.02	16.21
62231	0.104	0.149	0.159	0.163	0.169	50.57	0.47	11.63	3.67	22.5	3.89	7.13	0.58	25.7	5.31	44.5	6.59	15.3
64801	0.102	0.175	0.187	0.191	0.199	53.59	0.55	12.16	3.76	24.38	3.74	7.45	0.63	26.5	4.82	44.6	6.09	15.6
67461	0.194	0.281	0.278	0.281	0.294	25.36	0.13	6.24	1.64	11.13	1.89	3.7	0.44	27.3	4.93	44.4	5.11	16.1
67481	0.164	0.235	0.237	0.24	0.25	27.57	0.21	7.06	1.54	12.21	1.8	4.16	0.49	26.7	5.19	44.7	5.98	15.6
70181	0.056	0.102	0.118	0.123	0.128	58.3	1.76	9.62	6.35	25.59	5.53	7.87	6.659	15.68	12.93	42.25	9.285	11.71
70181	0.051	0.08	0.088	0.089	0.092	51.7	1.59	8.84	5.43	22.7	4.89	6.82	8.031	12.94	15.8	41.17	10.16	10.6
70181	0.047	0.071	0.072	0.072	0.074	43.4	1.55	6.9	4.95	18.97	4.17	5.82	8.275	11.73	16.32	41.53	10.31	10.51
71501	0.046	0.085	0.099	0.102	0.105	53.1	1.3	8.44	6.05	23.42	6.21	6.27	8.434	14.79	13.77	41.2	8.933	11.42
71501	0.046	0.076	0.081	0.081	0.083	44.8	1.71	6.72	5.38	19.8	4.44	5.78	10.04	11.85	16.76	39.85	9.728	10.32
71501	0.047	0.075	0.074	0.072	0.073	38.3	1.13	5.44	4.25	17.16	4.06	5.36	10.91	10.13	18.14	39.14	10.16	10.13
79221	0.052	0.091	0.105	0.109	0.114	61.5	1.69	10.27	7.44	26.57	5.98	7.2	5.948	16.22	11.53	43.15	9.784	11.94
79221	0.043	0.068	0.071	0.071	0.074	54.3	1.32	9.67	5.86	23.89	5.27	6.79	7.345	13.14	15.28	41.67	10.59	10.59
79221	0.047	0.069	0.069	0.07	0.071	46.5	1.2	7.86	5.07	20.83	4.45	5.91	7.546	11.86	16.16	41.41	11.15	10.53

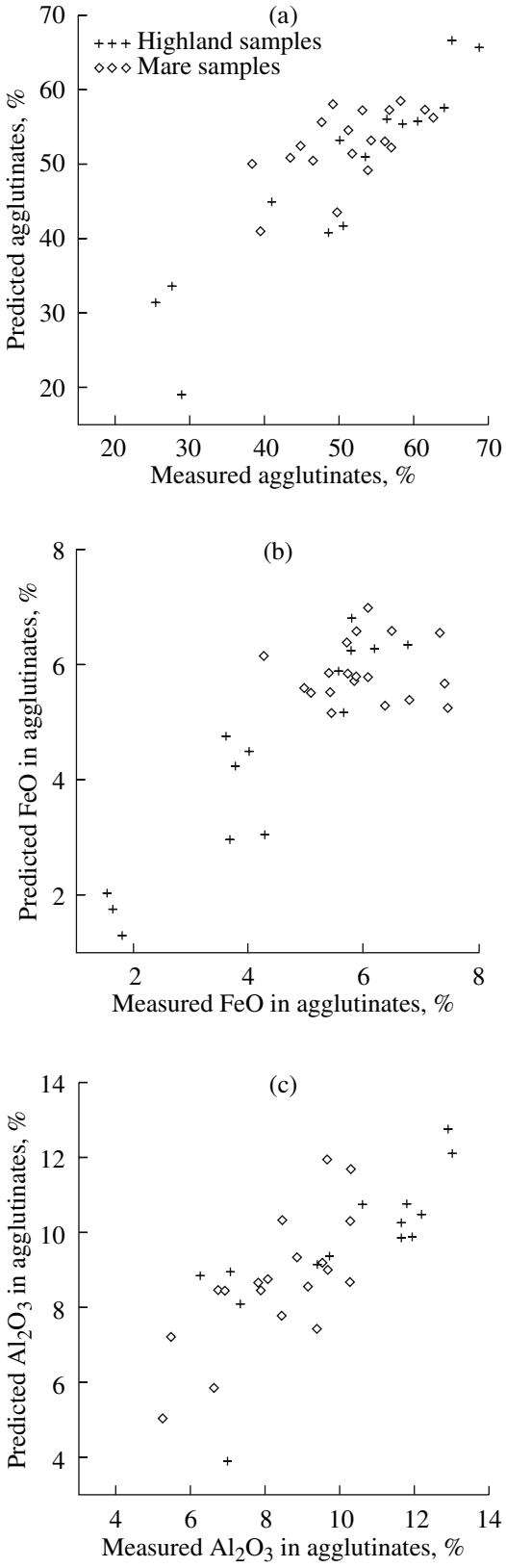

Fig. 2. The correlation diagrams (a) for the measured and predicted abundances of agglutinates (mass %), (b) for the FeO content in agglutinates, and (c) for the Al_2O_3 content in agglutinates.

MAPS OF THE AGGLUTINATE COMPOSITION

First of all, we built the prognosis map for the occurrence of agglutinates throughout the lunar surface. This map is given in Fig. 3a. As should be expected, the regions with the lowest abundance of agglutinates correspond to young craters (for example, the craters Tycho, Aristarchus, and others) and their ray systems. The prognosis of the distribution of the agglutinate abundance agrees well with the analogous map of the maturity degree I_s/FeO (Shkuratov et al., 2005b; Pieters et al., 2006). Weak variations of the agglutinate abundance are observed in the lunar maria. The pyroclastic areas, such as the plateau Aristarchus, are also prominent. The maps of the FeO and Al_2O_3 distributions are presented in Figs. 3a and 3b. As should be expected (see, e.g., Fischer and Pieters (1995) and Shkuratov et al. (2005b)), these distributions demonstrate an inverse correlation. The Al_2O_3 content map closely resembles the albedo map.

Figure 4a shows the distribution of the FeO content only in agglutinates, $FeO^{(agg)}$. In general, this content correlates with the bulk content of FeO. Analogously, Fig. 4b presents the distribution of Al_2O_3 in agglutinates, $Al_2O_3^{(agg)}$. In contrast to the previous case, this distribution rather resembles the map of agglutinate abundances (Fig. 3a). We analyzed the correlation between the maps of the FeO and Al_2O_3 contents in more detail. Figures 5a and 5b show the FeO–Al_2O_3 correlation diagrams for the bulk content and for the agglutinates, respectively. The crosses and diamonds correspond to the lunar soil samples; their distribution agrees rather well with the map data. The bulk contents of FeO and Al_2O_3 demonstrate a strong inverse correlation; the dependence is hyperbolic. For FeO and Al_2O_3 in agglutinates, the relation is more complex (Fig. 5b).

In order to ascertain whether there is any real excess of the FeO content in the highland agglutinates relative to that in maria, we built an image displaying the distribution of the $\dfrac{FeO^{(agg)}}{(FeO)G}$ ratio, where G is the abundance of agglutinates in the lunar surface (see Fig. 6a). It was found that such an excess is really observed. The heterogeneity of maria is almost not seen in Fig. 6a because of the normalization to the agglutinate abundance, correlating with the soil maturity, which reduces different surface regions to the same maturity.

The content of Al_2O_3 was analyzed in the same way. Figure 6b shows the map of the ratio of the Al_2O_3 content in agglutinates to the bulk content of Al_2O_3 and to the abundance of agglutinates on the lunar surface. The relative excess of the Al_2O_3 content in the mare agglutinates is globally observed. The normalization of the images shown in Figs. 6a and 6b to the agglutinate

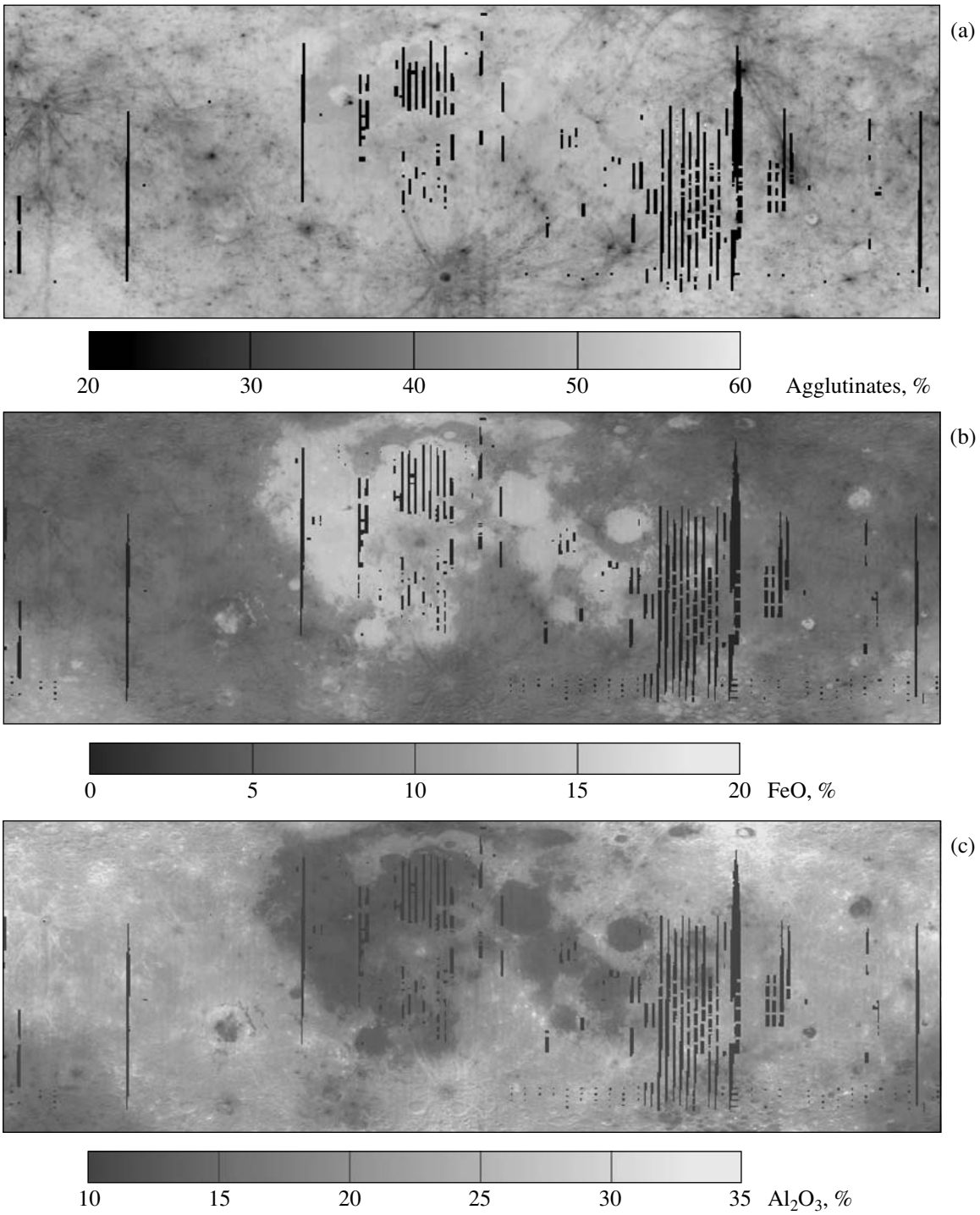

Fig. 3. The distribution of agglutinates (a) and the contents of FeO (b) and Al_2O_3 (c) over the lunar surface.

abundance allows us to compare the relative content of FeO and Al_2O_3 in agglutinates of soils of different maturity. In the maps of the $\frac{FeO^{(agg)}}{(FeO)G}$ and $\frac{Al_2O_3^{(agg)}}{(Al_2O_3)G}$ ratios (Figs. 6a and 6b), the ray systems of young craters are well seen. The relative content of FeO in the agglutinates of ray systems of the highland craters is higher, and the relative content of Al_2O_3 is lower than that in the agglutinates of the more mature soils surrounding the ray systems. This is connected with the normalization of the images in Figs. 6a and 6b to the bulk contents of FeO and Al_2O_3 that are, respectively, lower and higher in the ray systems than in the sur-

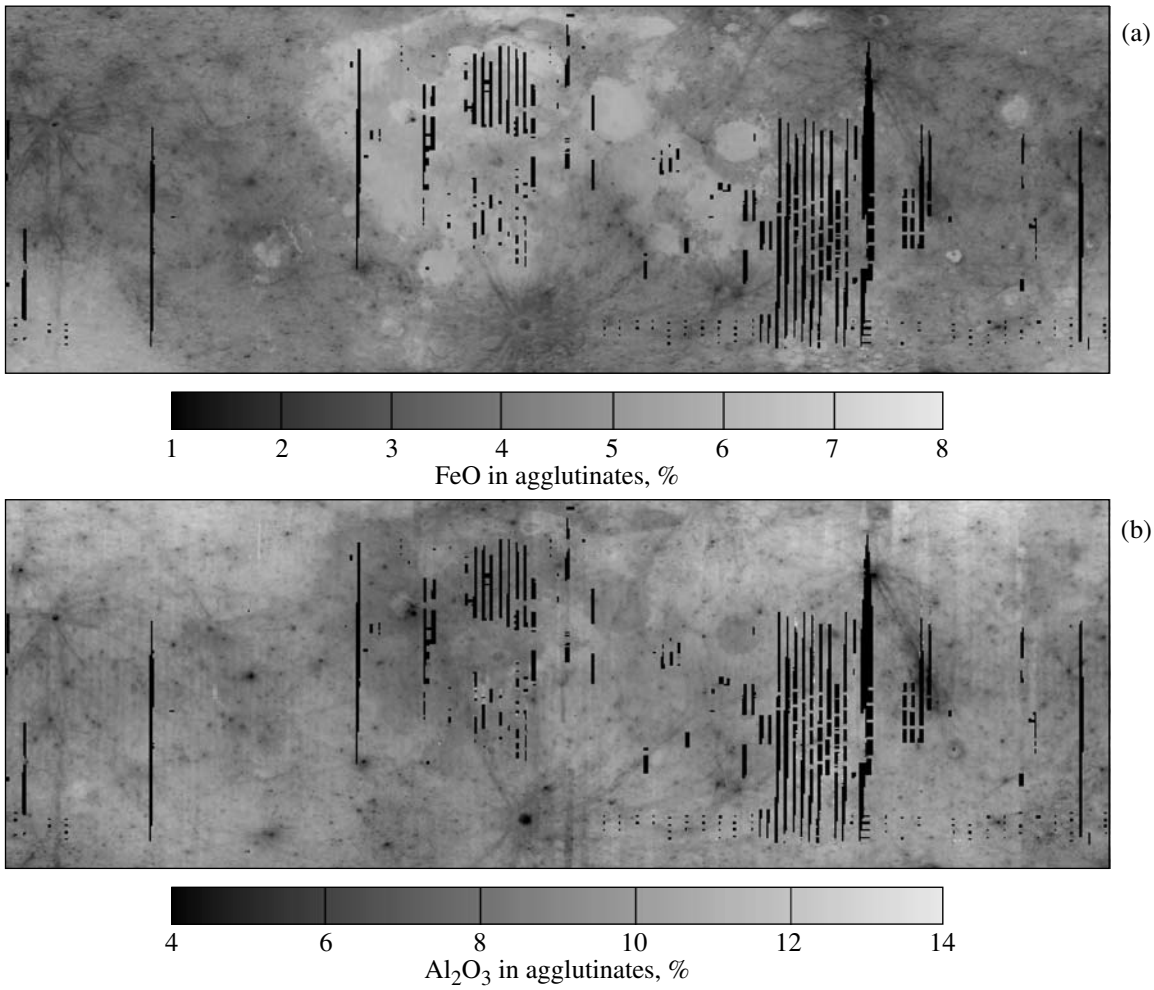

Fig. 4. The distribution of the contents of FeO (a) and Al_2O_3 (b) in agglutinates from the lunar surface.

rounding highland soil (Shkuratov et al., 2005a, 2005b).

THE MECHANISMS OF GLOBAL MATERIAL TRANSPORT

Evidence of global regolith mixing can be found while comparing the compositions of the lunar rocks and the regolith. The points corresponding to the highland and mare rocks are at the ends of the FeO–Al_2O_3 correlation diagram (Haskin and Warren, 1991), while the bulk contents of the regolith samples occupy the diagram area between mare and highland domains. The mare soil can be contaminated with the highland soil in two ways. The first is by way of vertical mixing: rather strong impact events may breach the mare lava cover and unseal the underlying highland material that mixes with the mare material. The second way is through horizontal transport, when the highland material is transported to the mare regions by impact ejecta. The horizontal transport also changes the composition of the highland material toward the mare material. Since the admixture of foreign matter must grow with exposure of the surface, one may expect that the mature soils deviate stronger from the local rocks in composition than the immature ones. This is confirmed by the prognosis maps of the FeO and Al_2O_3 content (Shkuratov et al., 2005a, 2005b): the ray systems are prominent there.

In other words, the highlands are contaminated with the mare material due to horizontal transport, while the maria can be contaminated with the highland material due to both vertical and horizontal transport. This circumstance may cause a poor correlation between the distributions of $FeO^{(agg)}$ and $Al_2O_3^{(agg)}$ shown in Figs. 4a and 4b (see also Fig. 5b). Now, we will consider the factors which might be related to the anomalies observed.

Table 2. The parameters of Eq. (1) and the correlation coefficient for the measured and predicted agglutinate abundances

	a	*b*	*c*	*d*	*E*	*k*
Agglutinates	–0.057	0.038	–0.078	0.065	1.782	0.85

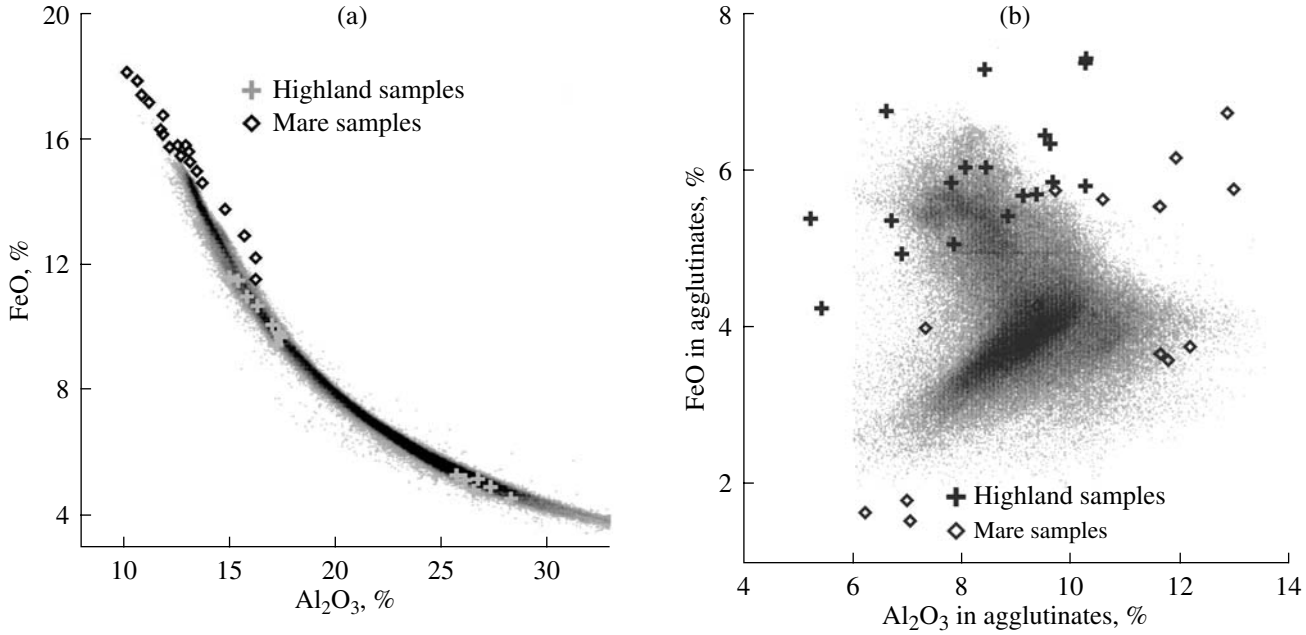

Fig. 5. The FeO–Al_2O_3 correlation diagrams for the bulk material (a) and agglutinates (b). The crosses and diamonds show data for the lunar soil samples.

Crater Ejecta. This mechanism of mixing of the mare and highland materials is the best studied. Almost all of the material from craters larger than 100 m across is transported in the form of rocks and blocks. Before coming into the agglutinates, they must be crumbled up. In the crumbling process, the rock material is mixed thoroughly with the local regolith to contribute to its bulk content, but this cannot produce an excess of these or those oxides in agglutinates. Owing to this mechanism, the above-mentioned small anomalies of the bulk content of FeO and Al_2O_3 in young highland craters and their ray systems can be explained: there is less FeO and more Al_2O_3 there, because these regions are less contaminated with mare material due to their young age.

Transport of Small Particles. Agglutinates are produced during the micrometeoritic bombardment. From the spectra of impactor masses (Lebedinets, 1981), it follows that 90% of agglutinates are produced due to the impacts of micrometeorites smaller than 1 mm in diameter (Starukhina and Shkuratov, 2004). Such impacts not only form the local regolith, but can also provide the long-range transport of regolith particles. Ejecta with initial velocities ranging from 1 km/s (which corresponds to the transport to distances of about 1000 km) to the escape velocity from the lunar surface (2.37 km/s) participate in global mixing. Such velocities are smaller than sonic speed in a solid substance. Therefore, the physical processes accompanying the secondary impacts differ from those taking place under supersonic impacts of the initial impactors with the Moon. A major difference is that in a high-velocity impact, an explosion occurs on the surface, while the result of a subsonic impact resembles that of the flight of a bullet penetrating into a solid or loose target. Such an impact may produce a hole in the solid material or a depression in the regolith without melting or evaporation. The particles of such ejecta penetrate into the regolith to the depth of several times its own size and contribute both to the bulk composition of the regolith and to the composition of the agglutinates. Moreover, if in a given surface region the ratio of agglutinates to the total number of particles is smaller than that for the incoming particles, the change of the rela-

Table 3. The correlation coefficients for the measured and predicted contents of some oxides in agglutinates and in the bulk samples

Oxides	Correlation coefficient for agglutinates	Correlation coefficient for the bulk content
FeO	0.83	0.90
Al_2O_3	0.76	0.87
CaO	0.81	0.90
TiO_2	0.59	0.68
MgO	0.90	0.89

Table 4. The parameters of Eq. (1) for estimating the FeO and Al_2O_3 contents in agglutinates and in the bulk samples

Oxides	*a*	*b*	*c*	*D*	*e*
FeO	–0.071	0.107	0.049	–0.130	1.361
FeO in agglutinates	–0.115	0.108	–0.021	–0.029	0.890
Al_2O_3	0.057	–0.085	–0.055	0.115	1.001
Al_2O_3 in agglutinates	–0.002	–0.033	–0.181	0.201	0.971

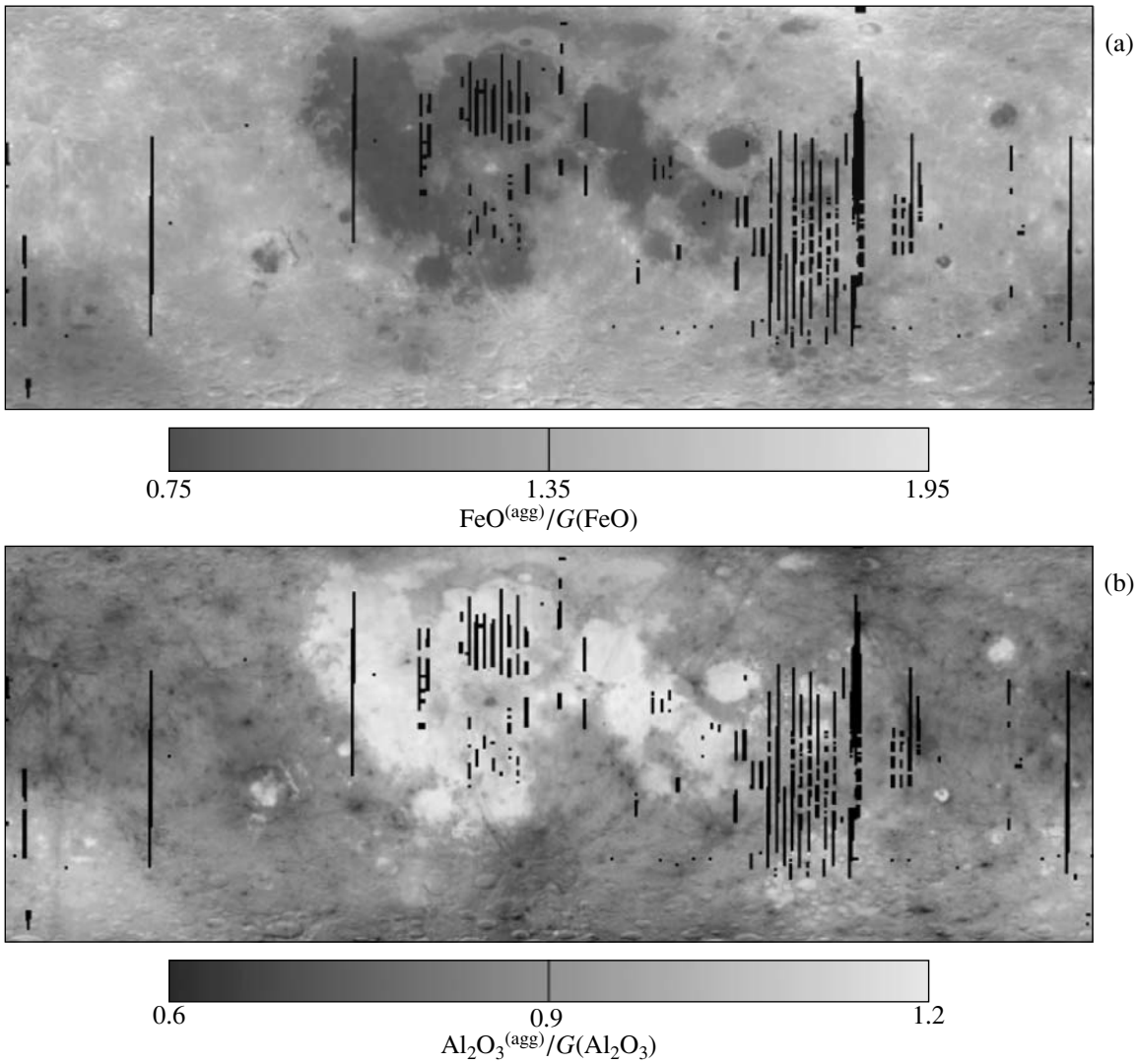

Fig. 6. The distribution of the ratio of the $FeO^{(agg)}$ content to the bulk content of FeO normalized to the portion of agglutinates in the soil G (a); the same but for Al_2O_3 (b).

tive composition of agglutinates in this particular region can be provided; i.e., this mechanism is effective for the areas covered with immature regolith. This mechanism could explain the anomalies in the $\frac{FeO^{(agg)}}{(FeO)G}$ and $\frac{Al_2O_3^{(agg)}}{(Al_2O_3)G}$ ratios observed in the ray systems of young craters (see Fig. 6).

Transport of Atoms Through the Lunar Exosphere. In addition to the material transport connected with meteoritic and micrometeoritic impacts, there are mechanisms of the atomic transport of material to large distances. These are the scattering and depositing of the products of impact evaporation in the meteoritic bombardment and the products of surface sputtering by the solar-wind ions. The contribution of these two mechanisms to the iron and aluminum exchange between maria and highlands was found to be substantial (Starukhina, 2003). The depositing of evaporated and sputtered atoms occurs on the surface of all particles, but the agglutinate particles were exposed statistically longer and, therefore, they accumulated more foreign matter.

CONCLUSIONS

The results of the present study are the prognosis maps of the agglutinate abundance and the FeO and Al_2O_3 contents in the lunar regolith. The maps were built with data from the UVVIS/*Clementine* imagery of the lunar surface and with the spectral, chemical, and mineral measurements of about 30 lunar soil samples. Our prognosis confirms that the mare agglutinates are enriched in Al_2O_3 and depleted of FeO, while the highland agglutinates are depleted of Al_2O_3 and enriched in FeO.

ACKNOWLEDGMENTS

The authors are grateful to L. Taylor for providing the data on the measurements of the laboratory samples, and to D.G. Stankevich and V.V. Omel'chenko for their help in the course of the study. Support from the CRDF grant (UKP2-2614-KH-04) is acknowledged.

REFERENCES

Fischer, E.M. and Pieters, C.M., Lunar Surface Aluminum and Iron Concentration from *Galileo* Solid State Imaging Data, and the Mixing of Mare and Highland Materials, *J. Geophys. Res.*, 1995, vol. 100, pp. 23279–23290.

Haskin, L. and Warren, P., Lunar Chemistry, *Lunar Sourcebook*, Heiken, G.H., Vaniman, D.T., and French, B.M., Eds., New York: Cambridge Univ. Press, 1991, Chap. 8, pp. 357–474.

Kaydash, V., Shkuratov Yu., Stankevich D., et al., Maps Characterizing the Lunar Regolith Maturity, *Lunar and Planet. Sci. Conf. 35th,* Houston: LPI, 2004, Abstract #1508.

Lebedinets, V.N., *Aerozol' v verkhnei atmosfere i kosmicheskaya pyl'* (Aerosol in the Upper Atmosphere and Cosmic Dust), Leningrad: Gidrometeoizdat, 1981.

McKay, D., Heiken, G., Basu, A., and Blanford, G., The Lunar Regolith, *Lunar Sourcebook*, Heiken, G.H., Vaniman, D.T., and French, B.M., Eds., New York: Cambridge Univ. Press, 1991, Chap. 7, pp. 285–356.

McEwen, A., Eliason, E., Lucey, P., et al., Summary of Radiometric Calibration and Photometric Normalization Steps for the *Clementine* UVVIS Images, *Lunar and Planet. Sci. Conf. 29th*, Houston: LPI, 1998, Abstract #1466.

Pieters, C.M. and Taylor, L.A., Systematic Global Mixing and Melting in Lunar Soil Evolution, *Geophys. Res. Lett.*, 2003, vol. 30(20), 2048. Doi: 10.1029/2003GL08212.

Pieters, C. and Hiroi, T., RELAB (Reflectance Experiment Laboratory): a NASA Multispectral Spectroscopy Facility, *Lunar and Planet. Sci. Conf. 35th*, Houston: LPI, 2004, Abstract #1720.

Pieters, C.M., Stankevich, D.G., Shkuratov, Yu.G., and Taylor, L.A., Statistical Analysis of the Links Between Lunar Mare Soil Mineralogy, Chemistry and Reflectance Spectra, *Icarus*, 2002, vol. 155, pp. 285–298.

Pieters, C., Shkuratov, Yu., Kaydash, V., et al., Lunar Soil Characterization Consortium Analyses: Pyroxene and Maturity Estimates Derived from Clementine Data, *Icarus,* 2006, vol. 184, pp. 83–101.

Rode, O., Ivanov, A., Nazarov, M., et al., *Atlas of Photomicrographs of the Surface Structures of the Lunar Regolith Particles*, Praha: Academia, 1979.

Shkuratov, Yu., Stankevich, D., Kaydash, V., et al., Composition of the Lunar Surface As Will Be Seen from SMART-1: A Simulation Using *Clementine* Data, *J. Geophys. Res., Ser. E*, 2003, vol. 108, no. 4, pp. 1–1 – 1–12.

Shkuratov, Yu., Kaydash, V., Stankevich, D., et al., Derivation of Elemental Abundance Maps at Intermediate Resolution from Optical Interpolation of Lunar Prospector Gamma-Ray Spectrometer Data, *Planet. Space Sci.*, 2005a, vol. 53, pp. 1287–1301.

Shkuratov, Yu.G., Kaydash, V.G., and Pieters, C.M., Lunar Clinopyroxene and Plagioclase: Surface Distribution and Composition, *Astron. Vestn.*, 2005b, vol. 39, no. 4, pp. 291–303 [*Sol. Syst. Res.* (Engl. Transl.), vol. 39, no. 4, pp. 255–366].

Starukhina, L.V., Computer Simulation of Sputtering of Lunar Regolith by Solar Wind Protons: Contribution to Change of Surface Composition and to Hydrogen Flux at the Lunar Poles, *Astron. Vestn.*, 2003, vol. 37, no. 1, pp. 36–50 [*Sol. Syst. Res.* (Engl. Transl.), vol. 37, no. 1, pp. 36–50].

Starukhina, L.V. and Shkuratov, Yu.G., Global Mixing As a Mechanism for Compositional Anomalies of Agglutinitic Glasses, *Lunar and Planet. Sci. Conf. 35th*, Houston: LPI, 2004, Abstract #1497.

Taylor, L.A., Pieters, C.M., Morris, R.V., et al., Lunar Mare Soils: Space Weathering and the Major Effects of Surface-Correlated Nanophase Fe, *J. Geophys. Res.,* 2001, vol. 106, pp. 27985–28000.

Taylor, L.A., Pieters, C.M., Patchen, A., et al., Mineralogical Characterization of Lunar Highland Soils, *Lunar and Planet. Sci. Conf. 34th*, Houston: LPI, 2003, Abstract #1774.